Faraday instability of a two-layer liquid film with a free upper surface

Andrey Pototsky[1] and Michael Bestehorn[2]

[1]*Department of Mathematics, Faculty of Science Engineering and Technology, Swinburne University of Technology, Hawthorn, Victoria 3122, Australia*
[2]*Department of Statistical Physics and Nonlinear Dynamics, Brandenburg University of Technology, 03044 Cottbus-Senftenberg, Germany*

We study the linear stability of a laterally extended flat two-layer liquid film under the influence of external vertical vibration. The first liquid layer rests on a vibrating solid plate and is overlaid by a second layer of immiscible fluid with deformable upper surface. Surface waves, excited as the result of the Faraday instability, can be characterized by a time-dependent relative amplitude of the displacements of the liquid-liquid and the liquid-gas interfaces. The in-phase displacements are associated with a zigzag (barotropic) mode and the antiphase displacement corresponds to the varicose thinning mode. We numerically determine the stability threshold in the vibrated two-layer film and compute the dispersion relation together with the decay rates of the surface waves in the absence of vibration. The in-phase and the antiphase displacements are strongly coupled in the vibrated system. The interplay between the Faraday and the Rayleigh-Taylor instabilities in the system with heavier fluid on top of a lighter fluid is analyzed.

I. INTRODUCTION

Classic Faraday instability [1] occurs when a deformable interface between two liquids or between a liquid and a gas is subjected to external vibration orthogonal to the interface. Sufficiently strong vibration destabilizes the flat interface, leading to the formation of standing surface waves. The phenomenon has received much attention in the past and has now been extensively studied for various geometries of the system, including two semi-infinite liquid phases [2], two liquid films of finite or infinite thickness confined between two solid plates [3–8], one finite thickness liquid layer, supported by a solid plate and exposed to a gas phase [9–18], and a single unsupported soaplike viscoelastic liquid film [19].

Recently, the interest in the Faraday instability in viscous fluids has been revived by a series of experiments focusing on the hydrodynamic instabilities in systems with flexible boundaries [20–22]. The authors have studied the response of liquid droplets floating on a viscous bath of a finite depth to an external vibration. The system therefore extends the classic Faraday instability to the case of two deformable interfaces (lower liquid-liquid and upper liquid-gas interfaces) and a moving contact line that plays the role of a flexible boundary. It was shown that beyond the onset of the instability, the system follows a slow dynamics, with the boundary of the droplet gradually reaching an equilibrium shape. This effect can be seen as mutual adaptation between the pressure of the Faraday waves and the capillary response of the droplet.

Motivated by these experiments, we present here a detailed theoretical study of the linear stability of a laterally extended flat two-layer liquid film with two deformable interfaces under external vertical vibration. Our results can be applied to predict the onset of the Faraday instability in floating droplets of sufficiently large volume, when the lateral size of the drop is much larger than its thickness. We analytically determine the stability condition and numerically solve the resulting generalized eigenvalue problem to obtain the exact location of the stability threshold in the space of system parameters. To connect our results with experimentally studied systems, we choose liquid parameters as in Refs. [20,21]. By analyzing the deformations of the two interfaces, we discuss different types of instability mode. The in-phase (antiphase) deformations correspond to the zigzag
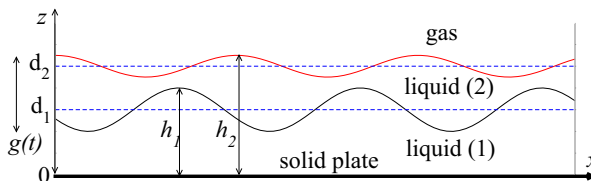
FIG. 1. Side view of the system in the comoving frame of the vertically oscillating solid bottom plate. Two immiscible fluids are separated by a deformable interface at $z = h_1(x,y,t)$. The deformed upper liquid-gas interface is located at $z = h_2(x,y,t)$. The nondeformed flat film has a width of d_1 (lower fluid) and d_2 (total thickness). The time-dependent acceleration in the comoving frame of the solid plate is $\boldsymbol{g}(t) = -g_0\boldsymbol{e}_z[1 + a\cos(\omega t)]$.

(varicose) mode. The zigzag mode is also referred to as the barotropic mode [21]. We apply our results to study the gravity-capillary surface waves in the vibration-free system and the Faraday instability in a two-layer film composed of a lighter fluid on top of the heavier fluid.

For liquid parameters chosen here we find that the zigzag surface wave is less stable than the varicose wave with the same wavelength, thus confirming experimental findings [21]. When the surface tension of the liquid-liquid interface is small compared with that of the upper film surface, the more stable varicose mode shows an anomalous dispersion relation with negative group velocity. When the system is vibrated at high frequency, the zigzag (varicose) mode becomes excited at low (large) vibration amplitudes. Finally, we study the interplay between the Faraday instability and the Rayleigh-Taylor instability in the system with heavier fluid on top of a lighter fluid. At low vibration frequencies we find isolated islands of instability in the space spanned by the wave vector and the vibration amplitude.

The paper is organized as follows. In Sec. II the Navier-Stokes equations in each layer together with the boundary conditions are reduced to a generalized eigenvalue problem with the eigenvector representing the deformations of the liquid-liquid and the liquid-gas interfaces. In Sec. III we switch off the vibration and obtain the dispersion relation of the surface gravity-capillary waves and the corresponding decay rates as a function of the wave vector. The Faraday instability is analyzed in Sec. IV and compared with the dispersion relation from Sec. III. The Rayleigh-Taylor unstable system, subjected to external vertical vibration, is studied in Sec. V.

II. LINEAR STABILITY OF A FLAT TWO-LAYER FILM UNDER VERTICAL VIBRATION

A. System

The side view of the system is shown in Fig. 1. In the comoving frame of the vertically oscillating solid substrate, the effective gravity acceleration is given by

$$\boldsymbol{g}(t) = -g(t)\boldsymbol{e}_z = -g_0(1 + a\cos\omega t)\boldsymbol{e}_z, \tag{1}$$

with $g_0 = 9.81$ m/s^2 and dimensionless acceleration amplitude a. Note that for $|a| < 1$ the effective acceleration $\boldsymbol{g}(t)$ is directed against the z axis, i.e., opposite to $\boldsymbol{e}_z$.

The densities of the fluids are ρ_i, $i = 1,2$, with $i = 1$ ($i = 2$) referring to the lower (upper) fluid. In the absence of vibration, the system is stable for $\rho_2 \leqslant \rho_1$ and it is Rayleigh-Taylor unstable for $\rho_2 > \rho_1$. A flat two-layer film corresponds to constant thicknesses of the fluids $h_1 = d_1$ and $h_2 = d_2$.

B. Linearized Navier-Stokes equations

Let $\boldsymbol{u}_i = [(u_x)_i,(u_y)_i]$ be the horizontal velocity and w_i the vertical velocity of the viscous and incompressible fluids in layer i, $i = 1,2$, in the comoving frame of the vibrating solid plate. The three-dimensional velocity of the fluids is then $\boldsymbol{v}_i = (\boldsymbol{u}_i,w_i)$ and the pressure in the ith layer is P_i.

In order to study the linear stability of a flat two-layer film, we linearize the Navier-Stokes equation in each layer about the base state, represented by the resting fluid, i.e., $\boldsymbol{u}_i = w_i = 0$,

$$\partial_t \boldsymbol{v}_i = \nu_i \nabla^2 \boldsymbol{v}_i - \frac{1}{\rho_i} \nabla P_i - g(t) \boldsymbol{e}_z, \tag{2}$$

with the kinematic viscosities of the fluids $\nu_i = \mu_i / \rho_i$, the three-dimensional nabla operator $\nabla = (\nabla_\parallel, \partial_z)$, and the horizontal nabla $\nabla_\parallel = (\partial_x, \partial_y)$.

Next we follow the procedure that was originally developed to study the Faraday instability in one-layer viscous films [9]. By applying twice the curl ($\nabla \times \nabla \times$) to both sides of Eq. (2) and using the continuity equations

$$\nabla_\parallel \cdot \boldsymbol{u}_i + \partial_z w_i = 0 \tag{3}$$

we eliminate the horizontal velocities $\boldsymbol{u}_i$ and the pressures P_i to obtain

$$\left[\partial_t - \nu_i \left(\nabla_\parallel^2 + \partial_z^2\right)\right]\left(\nabla_\parallel^2 + \partial_z^2\right) w_i = 0, \tag{4}$$

where w_i denotes the perturbed vertical velocity in the ith layer.

C. Boundary conditions

The unperturbed liquid-liquid and the liquid-gas interfaces are located at $z = d_1 = \text{const}$ and $z = d_2 = \text{const}$, respectively. When the vertical vibration sets in, both interfaces dynamically deform with the instantaneous thickness of the lower film h_1 and the total depth of the two-layer film h_2 given by

$$h_i(x, y, t) = d_i + \delta h_i(x, y, t), \tag{5}$$

with $|\delta h_i| \ll d_i$ in the linear regime.

At the deformed interfaces, the horizontal $\boldsymbol{u}_i$ and the vertical w_i velocities of the perturbed fluid satisfy the kinematic boundary conditions

$$\partial_t h_i + (\boldsymbol{u}_i \cdot \nabla_\parallel) h_i = w_i \quad [z = h_i(x, y, t)]. \tag{6}$$

Note that at $z = h_1(x, y, t)$ the velocities in both layers coincide

$$(\boldsymbol{u}_1, w_1) = (\boldsymbol{u}_2, w_2) \quad [z = h_1(x, y, t)]. \tag{7}$$

Linearizing Eq. (6) about the base state $h_i = d_i$ and $\boldsymbol{u}_i = w_i = 0$ and by Taylor expanding $\boldsymbol{u}_i$ and w_i around the unperturbed film thicknesses d_i, we obtain

$$\partial_t(\delta h_i) = w_i \quad (z = d_i), \tag{8}$$

$$\boldsymbol{u}_1 = \boldsymbol{u}_2 \quad (z = d_1), \quad w_1 = w_2 \quad (z = d_1). \tag{9}$$

At the solid plate, i.e., at $z = 0$ the fluid velocity vanishes, implying that

$$w_1(z = 0) = 0, \quad \partial_z w_1(z = 0) = 0. \tag{10}$$

Next we consider the boundary conditions for the liquid stress tensors $\pi_{ln}^{(i)}$ ($l, n = x, y, z$) in the ith layer. At the liquid-gas interface $z = h_2(x, y, t)$, in the absence of external tangential stresses, the boundary conditions for the stress tensor are identical to those in Ref. [9]. For brevity, we skip the details of the derivation and state the final relations between w_2 and δh_2, as they appear at the constant level of $z = d_2$,

$$0 = \left(\nabla_\parallel^2 - \partial_z^2\right) w_2, \tag{11}$$

$$\hat{\boldsymbol{L}}_2 w_2 = [\rho_2 g(t) \nabla_\parallel^2 - \gamma_2 \nabla_\parallel^4](\delta h_2), \tag{12}$$

with the linear operator $\hat{\boldsymbol{L}}_2 = (\rho_2 \partial_t - \mu_2 \partial_z^2)\partial_z - 3\mu_2 (\nabla_\parallel^2)\partial_z$.

We proceed to derive the stress boundary conditions at the deformable liquid-liquid interface $z = h_1(x,y,t)$. The presence of a time periodic bulk force (acceleration due to vibration and gravity) modifies the stresses in the ith fluid according to

$$\boldsymbol{\pi}^{(i)} = \pi_{ln}^{(i)} = -P_i\delta_{ln} + \mu_i(\partial_l v_n + \partial_n v_l) - z\rho_i g(t)\delta_{lz}\delta_{nz} + C_i(x,y,t)\delta_{lz}\delta_{nz}, \tag{13}$$

where the inclusion of z-independent functions $C_i(x,y,t)$ is necessary due to the presence of the deformable interfaces. Note that Eq. (13) is consistent with the Navier-Stokes equations in each layer, namely, Eq. (2) can also be written as $\partial_t \boldsymbol{v}_i = \boldsymbol{\nabla} \cdot \boldsymbol{\pi}^{(i)}$ [23].

The function C_2 is obtained from the normal component of the stress tensor at $z = h_2(x,y,t)$ and is given by $C_2 = \rho_2 g(t) h_2(x,y,t)$. The function C_1 will be determined below from the respective boundary condition at $z = h_1$.

At $z = h_1(x,y,t) = d_1 + \delta h_1(x,y,t)$, we require the continuity of the tangential and normal components of the stresses in each layer. Using the continuity equation (3) and retaining only linear terms of the order of w_i, $\boldsymbol{u}_i$, and δh_i, we obtain for arbitrary height z, anywhere close to $z = h_1$,

$$0 = \mu_1\big(\nabla_\parallel^2 - \partial_z^2\big)w_1 - \mu_2\big(\nabla_\parallel^2 - \partial_z^2\big)w_2, \tag{14}$$

$$\gamma_1\nabla_\parallel^2 h_1 = P_2(z) - P_1(z) + C_1 - \rho_1 g(t)z - \rho_2 g(t)(h_2 - z) + 2\mu_1\partial_z w_1 - 2\mu_2\partial_z w_2. \tag{15}$$

The function C_1 can now be determined from Eq. (15) by requiring that in the resting fluid the pressure difference $P_2(h_1) - P_1(h_1)$ at $z = h_1$ is due to the Laplace pressure. This yields

$$C_1 = \rho_1 g(t) h_1 + \rho_2 g(t)(h_2 - h_1). \tag{16}$$

In order to derive the conditions for w_i and δh_i at the constant height of $z = d_1$ from Eqs. (14) and (15), we proceed as in Ref. [9]. First, we Taylor expand all functions in Eqs. (14) and (15) about $z = d_1$. Then we apply $\nabla_\parallel^2$ in Eq. (15) and $\boldsymbol{\nabla}_\parallel$ in Eq. (2). This allows us to eliminate the pressure difference $\nabla_\parallel^2(P_2 - P_1)$ and we obtain, similar to Eq. (12),

$$\hat{\boldsymbol{L}}_1 w_1 - \hat{\boldsymbol{L}}_2 w_2 = (\rho_1 - \rho_2)g(t)\nabla_\parallel^2(\delta h_1) - \gamma_1\nabla_\parallel^4(\delta h_1), \tag{17}$$

with $\hat{\boldsymbol{L}}_1 = (\rho_1\partial_t - \mu_1\partial_z^2)\partial_z - 3\mu_1(\nabla_\parallel^2)\partial_z$.

D. Linear stability condition as a generalized eigenvalue problem

The onset of the Faraday instability corresponds to a bounded (time-periodic or nonperiodic) solution of the linearized equation (2) with the boundary conditions derived above. Using the Floquet theory, we represent the perturbations w_i and δh_i according to

$$w_i = e^{\lambda t}\sum_{n=-\infty}^{\infty}\int_{-\infty}^{\infty}d\boldsymbol{k}\, w_i^{(n)}(z,\boldsymbol{k})e^{I\omega nt/2}e^{-I\boldsymbol{k}\cdot\boldsymbol{r}},$$

$$\delta h_i = e^{\lambda t}\sum_{n=-\infty}^{\infty}\int_{-\infty}^{\infty}d\boldsymbol{k}(\delta h)_i^{(n)}(\boldsymbol{k})e^{I\omega nt/2}e^{-I\boldsymbol{k}\cdot\boldsymbol{r}}, \tag{18}$$

with $I = \sqrt{-1}$, the two-dimensional position vector $\boldsymbol{r} = (x,y)$, and wave vector $\boldsymbol{k} = (k_x,k_y)$.

Any bounded solution corresponds to an imaginary Floquet exponent λ, i.e., $\mathrm{Re}(\lambda) = 0$, that falls in the interval $0 \leqslant \lambda \leqslant I\omega/2$. The values of $\lambda = 0$ and $\lambda = I\omega/2$ correspond to harmonic (with the period $T = 2\pi/\omega$) and subharmonic (with the period $2T = 4\pi/\omega$) periodic solutions. Any Floquet exponent of the form $\lambda = (n/m)I\omega$ with arbitrary integers $m > 2n$ corresponds to periodic solutions and any other imaginary Floquet exponent $\lambda \neq (n/m)I\omega$ gives rise to nonperiodic bounded solutions. As it will be shown below, the stability threshold of the Faraday instability always corresponds to the choice of $\lambda = 0$, which implies that only harmonic or subharmonic perturbations are excited.

To ensure the reality of w_i and δh_i for $\lambda = 0$, the complex expansion amplitudes satisfy $[w_i^{(n)}(z,\boldsymbol{k})]^* = w_i^{(-n)}(z,-\boldsymbol{k})$ and $[(\delta h)_i^{(n)}(\boldsymbol{k})]^* = (\delta h)_i^{(-n)}(-\boldsymbol{k})$, where asterisks denote complex conjugation. Substitution of Eqs. (18) into Eq. (4) results in a fourth-order differential equation for the amplitudes $w_i^{(n)}(z,\boldsymbol{k})$,

$$0 = \left(\lambda + \frac{I\omega n}{2} - \nu_i(\partial_z^2 - k^2)\right)(\partial_z^2 - k^2)w_i^{(n)}. \tag{19}$$

For any $\lambda + I\omega n/2 \neq 0$ the solution of Eq. (19) can be written in the form

$$\begin{aligned}
w_1^{(n)} &= W_1^{(n)}e^{kz} + W_2^{(n)}e^{-kz} + W_3^{(n)}e^{q_1 z} + W_4^{(n)}e^{-q_1 z}, \\
w_2^{(n)} &= W_5^{(n)}e^{kz} + W_6^{(n)}e^{-kz} + W_7^{(n)}e^{q_2 z} + W_8^{(n)}e^{-q_2 z},
\end{aligned} \tag{20}$$

with $q_i^2 = k^2 + I\omega n/2\nu_i + \lambda/\nu_i$.

Note that Eq. (20) is only valid for viscous fluids, i.e., for $\nu_i \neq 0$. The inviscid case $\nu_{1,2} = 0$ or the partly inviscid case, when only one of the fluids is ideal, is not addressed here.

The eight-component vector $\boldsymbol{W}^{(n)} = (W_1^{(n)}, \ldots, W_8^{(n)})$ can be expressed as a linear combination of $(\delta h)_1^{(n)}$ and $(\delta h)_2^{(n)}$, by substituting Eq. (20) into the boundary conditions (3), (8)–(11), and (14),

$$\begin{aligned}
w_1^{(n)} &= 0 \quad (z = 0), \\
\partial_z w_1^{(n)} &= 0 \quad (z = 0), \\
w_1^{(n)} &= w_2^{(n)} \quad (z = d_1), \\
\partial_z w_1^{(n)} &= \partial_z w_2^{(n)} \quad (z = d_1), \\
\mu_1(k^2 + \partial_z^2)w_1^{(n)} &= \mu_2(k^2 + \partial_z^2)w_2^{(n)} \quad (z = d_1), \\
w_1^{(n)} &= \left(\lambda + \frac{I\omega n}{2}\right)(\delta h)_1^{(n)} \quad (z = d_1), \\
(k^2 + \partial_z^2)w_2^{(n)} &= 0 \quad (z = d_2), \\
w_2^{(n)} &= \left(\lambda + \frac{I\omega n}{2}\right)(\delta h)_2^{(n)} \quad (z = d_2).
\end{aligned} \tag{21}$$

The solution of Eq. (21) has the form

$$\boldsymbol{W}^{(n)} = \boldsymbol{D}(\delta h)_1^{(n)} + \boldsymbol{E}(\delta h)_2^{(n)}, \tag{22}$$

with two eight-component vectors $\boldsymbol{D}$ and $\boldsymbol{E}$, which satisfy the matrix equations

$$\boldsymbol{M}\boldsymbol{D} = \left(\lambda + \frac{I\omega n}{2}\right)\delta_{\alpha,6}, \quad \boldsymbol{M}\boldsymbol{E} = \left(\lambda + \frac{I\omega n}{2}\right)\delta_{\alpha,8}, \tag{23}$$

with $\delta_{\alpha,6} = (0,0,0,0,0,1,0,0)$ and $\delta_{\alpha,8} = (0,0,0,0,0,0,0,1)$ and the 8×8 matrix $\boldsymbol{M}$ given in the Appendix.

Static deformations of the film interfaces do not induce any static fluid velocity. This implies that for $\lambda + I\omega n/2 = 0$, the solution of Eq. (19) is given by $w_i^{(0)}(z) = 0$ or, equivalently, $\boldsymbol{D} = \boldsymbol{E} = 0$.

We remark that for any $\lambda + I\omega n/2 \neq 0$, the vectors $\boldsymbol{D}$ and $\boldsymbol{E}$ can be found analytically by using, for example, the MAPLE analytic solver. However, due to the extremely lengthy algebra, we opt for the numerical solution of Eq. (23). In particular, we use the LAPACK package to solve Eq. (23) for each mode n. After the vectors $\boldsymbol{D}$ and $\boldsymbol{E}$ are found, we substitute Eqs. (20) and (22) into Eqs. (17)

and (12) to obtain the following recursive relation for $(\delta h)_i^{(n)}$:

$$A_{11}^{(n)}(\delta h)_1^{(n)} + A_{12}^{(n)}(\delta h)_2^{(n)} = -\frac{a(\rho_1 - \rho_2)g_0 k^2}{2}\big[(\delta h)_1^{(n+2)} + (\delta h)_1^{(n-2)}\big],$$

$$A_{21}^{(n)}(\delta h)_1^{(n)} + A_{22}^{(n)}(\delta h)_2^{(n)} = -\frac{a\rho_2 g_0 k^2}{2}\big[(\delta h)_2^{(n+2)} + (\delta h)_2^{(n-2)}\big], \tag{24}$$

with the coefficients $A_{ik}^{(n)}$ ($i,k = 1,2$) given in the Appendix.

Numerically, we truncate Eqs. (18) by introducing the total number of Fourier modes $-N \leqslant n \leqslant N$ and rewrite Eq. (24) as the generalized eigenvalue problem

$$\begin{pmatrix} A_{11}^{(n=-N,...,N)} & A_{12}^{(n=-N,...,N)} \\ A_{21}^{(n=-N,...,N)} & A_{22}^{(n=-N,...,N)} \end{pmatrix} \begin{pmatrix} (\delta h)_1^{(n=-N,...,N)} \\ (\delta h)_2^{(n=-N,...,N)} \end{pmatrix}$$

$$= -\frac{ag_0 k^2}{2} \begin{pmatrix} (\rho_1 - \rho_2)\boldsymbol{\Delta} & 0 \\ 0 & \rho_2\boldsymbol{\Delta} \end{pmatrix} \begin{pmatrix} (\delta h)_1^{(n=-N,...,N)} \\ (\delta h)_2^{(n=-N,...,N)} \end{pmatrix} \tag{25}$$

with the $[(2N + 1) \times (2N + 1)]$-dimensional block

$$\boldsymbol{\Delta} = \begin{pmatrix} 0 & 0 & 1 & 0 & 0 & 0 & \cdots \\ 0 & 0 & 0 & 1 & 0 & 0 & \cdots \\ 1 & 0 & 0 & 0 & 1 & 0 & \cdots \\ 0 & 1 & 0 & 0 & 0 & 1 & \cdots \\ \cdots & \cdots & \cdots & \cdots & \cdots & \cdots & \cdots \end{pmatrix}, \tag{26}$$

the diagonal $[(2N + 1) \times (2N + 1)]$-dimensional blocks $A_{ik}^{(n=-N,...,N)}$, and the eigenvalue $ag_0 k^2/2$. In what follows, we choose $N = 25$ and check the accuracy of the results by increasing the number of modes to $N = 50$.

For a fixed wave vector k and a fixed Floquet exponent λ from the interval $\lambda \in [0, I\omega/2]$ we set up the coefficients $A_{ik}^{(n)}$ by numerically computing the vectors $\boldsymbol{D}$ and $\boldsymbol{E}$ for each n. Subsequently, the LAPACK routine GGEV is used to solve the generalized eigenvalue problem Eq. (25). Only real values of the dimensionless acceleration amplitude a have physical meaning. The solution of Eq. (25) is symmetric with respect to $a \to -a$.

Our numerical results support the conclusion of Ref. [9], namely, that at the threshold of the Faraday instability only periodic perturbations with the period of either $T = 2\pi/\omega$ (harmonic) or $2T = 4\pi/\omega$ (subharmonic) are excited. All other bounded solutions of the eigenvalue problem (24) correspond to a complex-valued vibration amplitude a and thus cannot be considered as physically plausible. For each set of system parameters we numerically check this statement by solving Eq. (24) for 100 different values of the Floquet exponent λ from the interval $\lambda \in [0, I\omega/2]$. For parameters considered here, the real eigenvalues are only found for $\lambda = 0$ (or for $\lambda = I\omega/2$).

The validity of the semianalytic approach presented here is further tested by comparing the results with the analytically known stability threshold for the one-layer film [9]. Namely, for $\rho_1 = \rho_2$, $\mu_1 = \mu_2$, and $\sigma_1 = 0$, the two fluids are identical and the solution of the eigenvalue problem (25) has to exactly coincide with the corresponding solution found for the one-layer case [9]. We conducted the tests for different values of the fluid density and viscosity and found perfect agreement with the one-layer theory (details not shown).

III. DISPERSIVE SURFACE WAVES IN A TWO-LAYER LIQUID FILM

We begin with the analysis of the dispersion relation of surface waves in the vibration-free system, i.e., $a = 0$. The complex growth rate $\lambda = \lambda(\boldsymbol{k})$ of a surface wave with the wave vector $\boldsymbol{k}$ can be found from Eq. (24) by setting $a = 0$ and $\omega = 0$ in Eqs. (18), (23), (A1), and (A2). In this case, Eq. (24) transforms into a homogeneous system of two linear equations for the complex displacement

amplitudes $(\delta h)_i = \int_{-\infty}^{\infty} d\boldsymbol{k}(\delta h)_i(\boldsymbol{k})e^{\lambda t}e^{-I\boldsymbol{k}\cdot\boldsymbol{r}}$,

$$
\begin{pmatrix} A_{11}^{(\omega=0)} & A_{12}^{(\omega=0)} \\ A_{21}^{(\omega=0)} & A_{22}^{(\omega=0)} \end{pmatrix} \begin{pmatrix} (\delta h)_1 \\ (\delta h)_2 \end{pmatrix} = 0, \tag{27}
$$

where the coefficients $A_{ik}^{(\omega=0)}$ are from Eq. (A2) by setting $\omega = 0$. The solvability condition of Eq. (27) reads

$$
A_{11}^{(\omega=0)} A_{22}^{(\omega=0)} - A_{12}^{(\omega=0)} A_{21}^{(\omega=0)} = 0. \tag{28}
$$

For any fixed wave vector $\boldsymbol{k}$, the decay rate of the surface wave $\mathrm{Re}(\lambda)$ and its oscillation frequency $\mathrm{Im}(\lambda)$ are found from Eq. (28).

Additionally, we introduce the mode type of the wave, by considering the relative phase of the displacements at the liquid-liquid $(\delta h)_1$ and the liquid-gas $(\delta h)_2$ interfaces

$$
\frac{(\delta h)_2}{(\delta h)_1} = \frac{|(\delta h)_2|}{|(\delta h)_1|} \exp(I\,\Delta\phi) = -\frac{A_{11}^{(\omega=0)}}{A_{12}^{(\omega=0)}}, \tag{29}
$$

with the phase shift $\Delta\phi = \arctan\{\mathrm{Im}[(\delta h)_2/(\delta h)_1]/\mathrm{Re}[(\delta h)_2/(\delta h)_1]\}$. For vanishingly small $\Delta\phi \approx 0$, the displacements at the two interfaces are in phase, corresponding to a zigzag (barotropic) mode. For $\Delta\phi \approx \pi$, the displacements are in antiphase, giving rise to the varicose thinning mode. The relative amplitudes of the displacements are controlled by the ratio $\frac{|(\delta h)_2|}{|(\delta h)_1|}$. The notion of the mode type was introduced earlier by us in connection with the long-wave instabilities in ultrathin two-layer liquid films [24,25]. The barotropic zigzag mode was studied for droplets floating on a liquid bath in Ref. [21].

In order to make a connection with experimentally studied systems, we choose all liquid parameters as in Refs. [20–22] and consider a 1.9-mm-thick isopropanol film with low viscosity $\mu_2 = 0.0018$ Pa s, deposited on top of a 5-mm-thick perfluorated oil film with $\mu_1 = 0.026$ Pa s. The lower fluid is much heavier $\rho_1 = 1850$ kg/m^3 than the upper fluid with $\rho_2 = 785$ kg/m^3. The surface tensions at the liquid-liquid and the liquid-gas interfaces are $\gamma_1 = 0.0063$ N/m and $\gamma_2 = 0.024$ N/m, respectively. Figure 2(a) shows the imaginary part of the growth rate λ of a surface wave as a function of the wave number k. The corresponding (negative) decay rates $-\mathrm{Re}(\lambda)$ are given in Fig. 2(b).

We find that very long waves with $k < 0.002$ mm^{-1}, i.e., longer than $\Lambda = 2\pi/k \approx 3$ m, are nondispersive waves that decay monotonically. This is in agreement with the long-wave theory [24,25] that predicts monotonic gravity-capillary waves in two-layer liquid films. For $k < 0.002$ mm^{-1}, the least stable wave with the smallest decay rate is of the varicose type, as schematically shown in one of the insets in Fig. 2(b). As k increases, the first mode that becomes dispersive at $k = 0.002$ mm^{-1} is the zigzag mode, represented by the dashed lines in Figs. 2(a) and 2(b).

In the narrow window of the wave vectors $k \in [0.002, 0.013]$ mm^{-1}, the dispersive zigzag mode coexists with two different monotonically stable modes (solid line and dash-dotted lines). The least stable mode is as before the nondispersive varicose mode [lower nondispersive branch in Fig. 2(b)]. The more stable monotonic branch (upper nondispersive branch) represents a zigzag mode for small k that turns into a varicose mode at some critical k, marked by the circle in Fig. 2(b). The transition from a zigzag mode to a varicose mode occurs when the liquid-gas interface becomes flat.

For $k > 0.013$ mm^{-1} both branches are dispersive. The least stable mode is now of the zigzag type (dashed line). The relative deflection amplitudes $|\delta h_2/\delta h_1|$ and the phase shifts $\Delta\phi = \pi$ are shown for the dispersive branches only in Figs. 2(c)–2(e) with the line coding as in Figs. 2(a) and 2(b).

For the chosen parameters we find that both the zigzag mode and the varicose mode follow a normal dispersion relation with monotonically increasing $\mathrm{Im}(\lambda)$ as a function of k. Very short waves with $k > 1$ mm^{-1} propagate almost exclusively at either the liquid-gas or the liquid-liquid interface, as shown in the insets in Fig. 2(a). The least stable mode has an almost flat liquid-liquid interface.
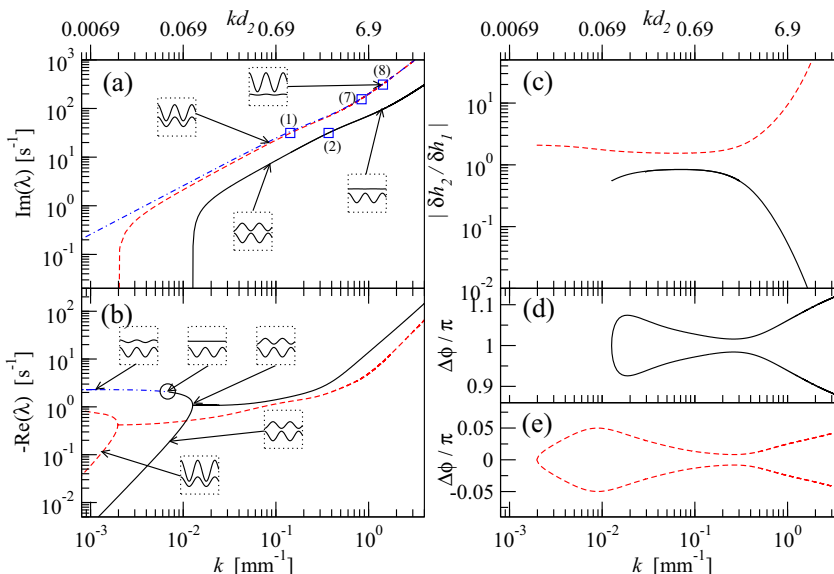
FIG. 2. (a) Dispersion relation of two types of surface waves in 1.9-mm-thick isopropanol film deposited on top of 5-mm-thick perfluorated oil film with the parameters taken from [22]: $\rho_1 = 1850 \, \text{kg/m}^3$, $\rho_2 = 785 \, \text{kg/m}^3$, $\gamma_1 = 0.0063$ N/m, $\gamma_2 = 0.024$ N/m, $\mu_1 = 0.026$ Pa s, and $\mu_2 = 0.0018$ Pa s. The upper branch (dashed line) corresponds to least stable zigzag mode and the lower branch (solid line) represents the faster decaying varicose mode. Four insets schematically show relative surface deformations for selected points on each branch. Open squares indicate the location of selected points, as in Fig. 4. Dash-dotted line corresponds to the dispersion curve of the gravity-capillary waves on the surface of a one-layer liquid film (30). (b) Negative decay rates $-\text{Re}(\lambda)$ of the two modes in (a). (c) Relative amplitude of the deflections at the liquid-liquid and the liquid-gas interfaces $|\delta h_2 / \delta h_1|$. Also shown are the phase shift $\Delta \phi$ from Eq. (29) in units of π for (d) the varicose mode and (e) the zigzag mode.

We compare the dispersion relation of the dominant zigzag mode with the analytically known dispersion curve $\Omega(k)$ of the gravity-capillary waves on the surface of a relatively thick one-layer liquid film [26]. For a liquid film with thickness h, fluid density ρ, and surface tension σ the latter is given by

$$\Omega(k)^2 = \left(g_0 k + \frac{\sigma k^3}{\rho} \right) \tanh(kh). \tag{30}$$

The dispersion curve $\Omega(k)$ is shown by the dash-dotted line in Fig. 2(a) for $\sigma = \sigma_2 = 0.024$ N/m, $\rho = \rho_2 = 785$ kg/m^3, and $h = 6.9$ mm. For $k > 10^{-1}$ mm^{-1} the one-layer analytic result (30) is almost indistinguishable from the numerically computed zigzag dispersion curve for the two-layer film.

These results are consistent with the experimental observations [21], reporting the domination of the zigzag (or barotropic) mode for the chosen fluid parameters. Note that an approximate analytic form of the dispersion relation of the zigzag mode [dashed line in Fig. 2(a)] was derived in Ref. [21] under the assumption that the standing wave is of a pure zigzag type with negligibly small decay rate. The approximation, derived in Ref. [21], coincides with Eq. (30) for an infinitely deep upper layer, i.e., for $\tanh(kh) \approx 1$. A more detailed relation of the dispersion curves in Fig. 2(a) to the onset of the Faraday instability will be presented in the next section.

Next we examine how the dispersion relations are effected by the surface tension of the liquid-liquid interface. For $\gamma_1 = 0.001$ N/m and all other parameters as in Fig. 2, the dispersion curve of the numerically found zigzag mode (dashed line in Fig. 3) coincides almost perfectly well with the
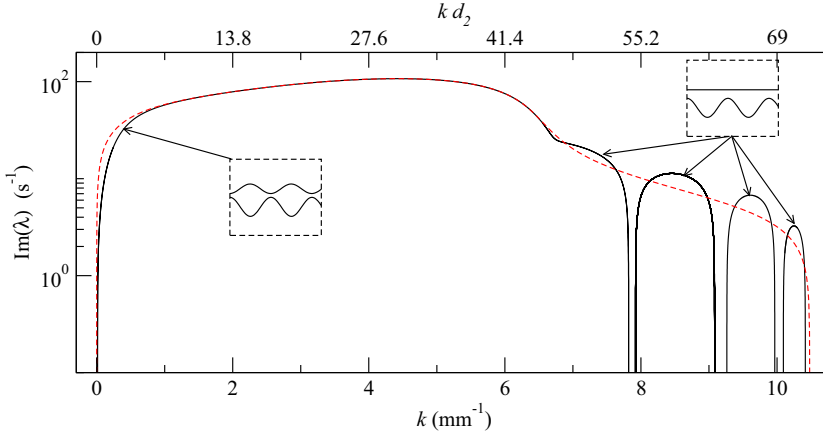
FIG. 3. (a) Anomalous dispersion curve of the varicose mode for a two-layer film with parameters as in Fig. 2 and $\gamma_1 = 0.001$ N/m. The solid line is the numerically computed frequency Im(λ) of the varicose mode from Eq. (28). The dashed line corresponds to the dispersion curve of the gravity-capillary waves at the interface between two semi-infinite viscous fluids, found numerically from Eq. (31).

dispersion relation of the gravity-capillary waves in a one-layer film from Eq. (30) (dotted line in Fig. 3). For the sake of simplicity, we only show in Fig. 3 the angular frequency Im(λ)(k) of the two dispersive modes, without discussing their respective decay rates.

The varicose mode shows an anomalous dispersion relation, with a nonmonotonic angular frequency Im(λ)(k) as a function of k, as given by the solid line in Fig. 3. We find that at $k \approx 4$ mm^{-1} the angular frequency Im(λ)(k) of the varicose mode starts to decrease, dropping to zero at around $k \approx 7.9$ mm^{-1}. At this point, the wave becomes nondispersive. The next dispersive branch is separated from the first branch by a narrow window of wave vectors, where the wave decays monotonically. In total we find four isolated branches of the dispersion curve between $k = 0$ and $k \approx 11$ mm^{-1}. For $k > 11$ mm^{-1} the waves decay monotonically with Im(λ) = 0.

The surface waves that correspond to the anomalous dispersion branch propagate at the liquid-liquid interface with the upper liquid-gas interface remaining almost flat, as shown in the insets in Fig. 3. In the case when one of the film interfaces is almost flat, the notion of the mode type becomes practically irrelevant.

In Fig. 3 we compare the dispersion relation of the varicose mode in a two-layer film with the dispersion relation of the gravity-capillary waves at the interface between two semi-infinite viscous fluids [6]. As it was shown in Ref. [6], the complex growth rate Λ_k of the interfacial waves can be found from the transcendental equation

$$0 = [\rho_1(k - Q_2) + \rho_2(k - Q_1)][(\rho_1 + \rho_2)\Lambda_k^2 + \omega_0^2(\rho_1 - \rho_2)]$$
$$- 4k[\rho_1\Lambda_k + k(\mu_1 - \mu_2)(k - Q_1)][\rho_2\Lambda_k - k(\mu_1 - \mu_2)(k - Q_2)], \qquad (31)$$

where $Q_i = k\sqrt{1 + \Lambda_k/\nu_i k^2}$ and $\omega_0^2 = g_0 k + \sigma_1 k^3/(\rho_1 - \rho_2)$.

We numerically solve Eq. (31) and plot the imaginary part of Λ_k by the dashed line in Fig. 3 for the two semi-infinite liquids with parameters as in Fig. 2 and $\sigma = 0.001$ N/m. The agreement between Im(Λ_k) and the dispersion curve of the two-layer film from Eq. (28) is remarkably good for all wave vectors k. In fact, in the case of two semi-infinite fluids, the interfacial waves also demonstrate an anomalous dispersion relation and become monotonically damped (nondispersive) for $k \gtrsim 11$ mm^{-1}.

In Ref. [6] the solution of Eq. (31) has been analyzed for two limiting cases: the so-called weak damping case that corresponds to $k \ll k_c$ and the strong damping case $k \gg k_c$, where the critical wave vector k_c can be estimated as $k_c \approx \sigma_1/(4(\rho_1 + \rho_2)v_2^2) = 18$ mm^{-1}. In the weak damping case the

waves behave as pure gravity waves with the dispersion relation $\text{Im}(\Lambda_k)^2 \approx g_0 k(\rho_1 - \rho_2)/(\rho_1 + \rho_2)$. In contrast, in the strong damping case the waves are monotonically damped with $\text{Im}(\Lambda_k) = 0$. Remarkably, however, the anomalous nature of the dispersion relation was not explicitly mentioned in Ref. [6].

The effect of the finite thickness of the layers and the presence of the deformable upper surface are reflected in the presence of the gaps of wave vectors in the dispersion relation, where the varicose mode is monotonically damped. As the thicknesses of both layers d_i are increased, the gaps narrow and eventually disappear. The dispersion curve in this limit converges to the dashed line in Fig. 3 (details not shown). Note that anomalous dispersion of surface waves was previously measured experimentally in one-layer ferromagnetic liquid films by making use of the Faraday instability [17].

IV. FARADAY INSTABILITY OF TWO-LAYER LIQUID FILMS

External vertical vibration leads to the excitation of the surface waves, found in Fig. 2. In fact, the Faraday instability can be seen as a resonance phenomenon in a continuous medium. Namely, when the acceleration amplitude a of the vibration is gradually increased, the first mode to become unstable is the one with the smallest decay rate.

In order to further characterize the parameter regimes selected here, we introduce two dimensionless parameters $L_1 = d_1/\sqrt{2\nu_1/\omega}$ and $L_2 = (d_2 - d_1)/\sqrt{2\nu_2/\omega}$ that measure the thickness of the liquid layers in relation to the corresponding acoustic length (i.e., $\sim \sqrt{2\nu_i/\omega}$ [9]) in each of the two fluids. If the thickness of the liquid layer is much larger than the acoustic length $\sqrt{2\nu/\omega}$, the lowest tongue of the Faraday instability is expected to be represented by the subharmonic excitations, as it was found for one-layer films [9]. For the two-layer films we expect a similar effect. In addition to L_1 and L_2, we supplement each figure with the alternative axis for the dimensionless wave vector kd_2, as in Fig. 2.

In Fig. 4 we plot the marginal stability threshold in variables (k,a) for two different vibration frequencies: $f = 10$ Hz [Fig. 4(a)] and $f = 50$ Hz [Fig. 4(b)] for the system with parameters as in Fig. 2. Selected frequencies correspond to $L_1 = 7.48$ and $L_2 = 7.03$ for $f = 10$ Hz and $L_1 = 16.72$ and $L_2 = 15.73$ for $f = 50$ Hz. Thus, we expect the lowest tongue to be subharmonic. Thin (thick) lines correspond to subharmonic (harmonic) tongues. For $f = 10$ Hz, the first mode to become unstable is marked by (1) in Fig. 4(a). The corresponding wave vector $k_{\min} = 0.14$ mm^{-1} exactly
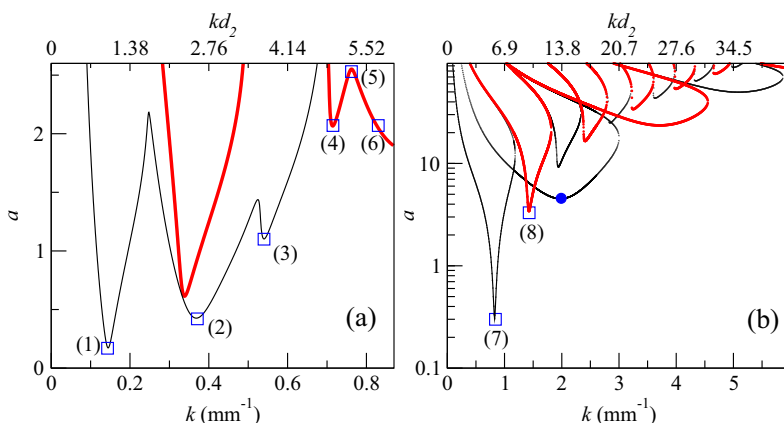

FIG. 4. Stability threshold of a flat two-layer film under vertical periodic vibration for (a) $f = 10$ Hz and (b) $f = 50$ Hz for the system as in Fig. 2. Thin (thick) lines correspond to subharmonic (harmonic) tongues. Selected points on the stability threshold (1), (2), (7), and (8) are also shown on the dispersion curves in Fig. 2(a).

falls onto the dispersion branch of the zigzag mode in Fig. 2(a) at half of the driving frequency $\text{Im}(\lambda) = 2\pi(f/2)$ rad/s, as marked by an open square.

The wave vector $k'_{\min} = 0.37$ at the second minimum of the marginal stability in Fig. 4(a), marked by (2), corresponds to the dispersion branch of the more stable varicose mode in Fig. 2(a). This allows to experimentally detect the more stable dispersion branch, as it was done in Ref. [17]. In this method, the amplitude a is gradually increased until the point $a = a_{\min}$, where the primary instability at $k_{\min} = 0.14$ [point (1)] sets in. Next, the amplitude is further increased until $a = a'_{\min}$, where the second wave with $k'_{\min} = 0.37$ is excited.

However, one should emphasize that this method can only be used when the amplitudes $a_{\min}$ and $a'_{\min}$ are relatively small. Thus, generically, according to Floquet theory, the amplitudes of the standing waves at the onset of the Faraday instability are given by periodic functions of time that are not necessarily sinusoidal, as stated in Eqs. (18). For small vibration amplitudes $a \ll 1$, the higher expansion modes in Eqs. (18) can be neglected so that the comparison with the vibration-free case (Fig. 2) can be established. However, if the onset amplitude is large, i.e., $a \gg 1$, the amplitudes of the standing surface waves at the onset of the instability are no longer given by sinusoidal functions of time, proportional to $e^{I \text{Im}(\lambda)t}$, and thus they cannot be compared with the dispersion curves in Fig. 2(a), which were obtained for sinusoidal oscillating surface waves.

In order to gain a deeper insight into the structure of the surface waves in two-layer films directly at the onset of the Faraday instability, we compute the eigenvectors of the generalized eigenvalue problem (24). For any fixed wave vector k, the real deformations of the liquid-liquid and the liquid-gas interfaces δh_i are found from Eqs. (18) and can further be written as

$$\delta h_i = \delta H_i(k,t)e^{-I k \cdot r} + \delta H_i^*(k,t)e^{I k \cdot r}, \tag{32}$$

with $\delta H_i(k,t) = \sum_{n=-N}^{N} (\delta h)_i^{(n)}(\boldsymbol{k}) e^{I \omega n t/2}$ for N Fourier modes.

Depending on the eigenvectors $(\delta h)_i^{(n)}$ ($-N \leqslant n \leqslant N$), the real functions in Eq. (32) capture both the standing and the traveling surface waves. However, for the parameters considered here, we only find standing waves that can be represented in the form

$$\delta h_i = F_i(t)\cos(kr + \phi), \tag{33}$$

where the time-independent phase ϕ is identical for δh_1 and δh_2. In what follows we normalize the time-dependent amplitudes $F_i(t)$ according to $\int_0^T F_i^2(t)dt = 1$.

We note that the form of the surface deformations in a two-layer liquid film is similar to the deformations of a vibrated viscoelastic sheet with two free interfaces [19]. In the latter case the deformations of the two surfaces of the sheet are also found to be either in phase (zigzag type or antisymmetric as in Ref. [19]) or in antiphase (varicose type or symmetric as in Ref. [19]).

Time-dependent amplitudes $F_i(t)$ from Eq. (33) are plotted over two periods of the forcing $2T = 4\pi/\omega$ in Fig. 5 for six selected points, marked by (1)–(6), on the threshold of the Faraday instability in Fig. 4(a). The points (1)–(3) correspond to the subharmonic deformations with the oscillation period of $2T$. For larger values of k the deformations are harmonic with the oscillation period T [points (4)–(6)].

One of the main conclusions that can be drawn from Fig. 5 is that the mode type of the excited standing wave changes over time. Thus, the vertical dotted lines in Fig. 5 correspond to the moments of time when one of the amplitudes $F_i(t)$ changes its sign. The varicose (zigzag) mode corresponds to a negative (positive) product $F_1 F_2$, as indicated by the letters v and z in Fig. 5, point (5).

It is instructive to compare the magnitudes of the amplitudes F_i for different positions on the stability threshold. Thus, the amplitudes F_i have similar magnitudes at points (1), (3), and (5). However, at points (2) and (6) the deformation of the liquid-liquid interface is at least one order of magnitude large than that of the liquid-gas interface. Conversely, at point (4), the surface wave is excited almost exclusively at the upper surface, with the liquid-liquid interface remaining almost flat.
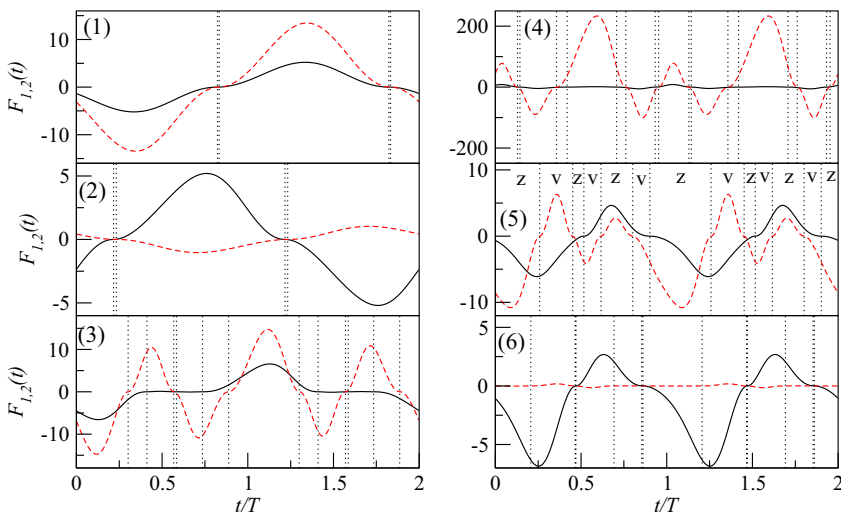
FIG. 5. Time-dependent amplitudes $F_{1,2}(t)$ of the standing Faraday waves for six selected points (1)–(6) on the stability threshold in Fig. 4(a): $F_1(t)$ (solid lines) and $F_2(t)$ (dashed lines). The amplitudes are normalized so that $\int_0^T F_1^2(t)dt = 1$. Vertical dotted lines indicate moments of time when the mode type changes between the varicose and the zigzag modes.

The results in Fig. 5 clearly show that the varicose and the zigzag modes are coupled in the vibrated two-layer film. In fact, for large vibration amplitudes, the structure of the excited surface waves is even more complicated since the type of mode changes over the oscillation cycle. The coupling of different mode types has previously been reported for unsupported soaplike viscoelastic films [19].

Next we examine how the stability threshold is effected by the frequency f of the external vibration. Thus, for a higher vibration frequency $f = 50$ Hz, the stability diagram changes qualitatively, as shown in Fig. 4(b). Now the second mode to become unstable, marked by (7), belongs to the harmonic tongue. In Figs. 6(a) and 6(b) we plot the onset amplitude $a_{\min}$ and the onset wave vector $k_{\min}$ as a function of the driving frequency f for parameters as in Fig. 2. For comparison, the curve $k_{\min}$ vs f (solid line) in Fig. 6(b) is compared with the dispersion curve of the zigzag mode in Fig. 2(a) at twice the oscillation frequency $f = \mathrm{Im}(\lambda)/\pi$ (dashed line). For $k > 0.5$ mm^{-1} the two curves are practically indistinguishable.

The onset amplitude $a_{\min}$ shows a nonmonotonic dependence on f, as given in Fig. 6(a): It decreases with f for small f, reaching a minimum at $f \approx 17$ Hz. At large driving frequencies $a_{\min}$ increases with f, in agreement with the experimental data for droplets floating on a high-viscosity liquid bath [17].

The behavior of the system is remarkable at extremely low driving frequencies $f < 0.5$ Hz. The marginal stability tongues are shown in Fig. 6(c) for $f = 0.4$ Hz and the rest of the parameters as in Fig. 2. At such a low frequency, the acoustic length in each layer is comparable to the layer thickness, i.e., $L_1 = 1.5$ and $L_2 = 1.4$. The least stable tongue is no longer the first but the eighth consecutive subharmonic tongue, marked by the open square. This feature of the stability diagram is similar to the Faraday instability in one-layer liquid films, as described in Ref. [9].

V. RAYLEIGH-TAYLOR INSTABILITY IN VERTICALLY VIBRATED TWO-LAYER LIQUID FILMS

When the upper fluid is heavier than the lower fluid, i.e., $\rho_2 > \rho_1$, the system is Rayleigh-Taylor unstable. Historically, the Rayleigh-Taylor instability was first studied theoretically in an unbounded system of two semi-infinite liquid phases, separated by a sharp interface [2]. Later extensions included
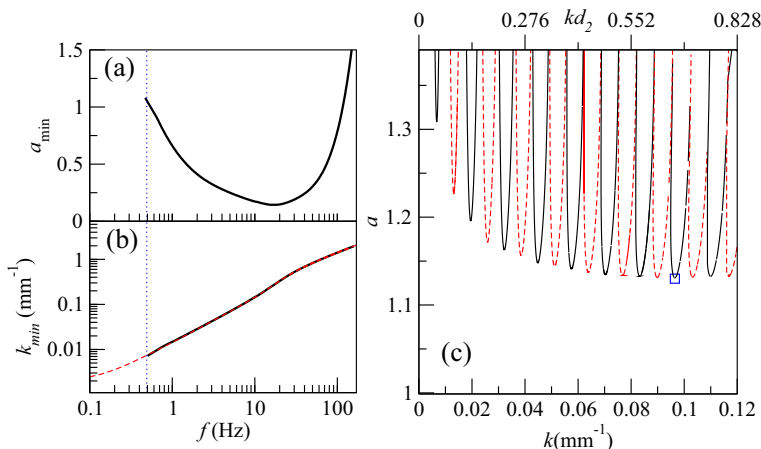
FIG. 6. (a) Onset vibration amplitude $a_{\min}$ and (b) onset wave vector $k_{\min}$ vs the driving frequency f for the system as in Fig. 2. Vertical dotted lines correspond to $f = 0.5$ Hz. The dashed line in (b) is the dispersion branch of the varicose mode [dashed line in Fig. 2(a)] at twice the oscillation frequency $f = \mathrm{Im}(\lambda)/\pi$. (c) Marginal stability tongues for $f = 0.4$ Hz: subharmonic (solid lines) and harmonic (dashed lines). The least stable mode is located at $k_{\min} = 0.096$ (mm^{-1}), as marked by the open square.

linear as well as nonlinear evolution of the interface between the fluids for different geometries of the system. Thus, a finite-thickness liquid film on top of a solid plate, overlaid by a heavier semi-infinite fluid phase, was discussed in Ref. [4]. Surface waves between two immiscible liquids confined in a two-dimensional channel were studied in Ref. [27]. In the case of a one-layer liquid film on the underside of a solid plate, the Rayleigh-Taylor instability was analyzed in Ref. [28].

Early experiments with two superimposed immiscible liquids and with a viscous liquid supported by air have demonstrated the possibility to stabilize the Rayleigh-Taylor instability of the interface between two phases by applying an external vertical vibration [7,29,30]. Theoretical analysis revealed that both the interfacial tension and the viscosity are necessary to stabilize the short-wave perturbations of the interface [8]. By applying the long-wave approximation, the vibration was shown to act as the surface tension, shrinking the band of linearly unstable wave vectors [5].

We are unaware of studies of the interplay between the Faraday and the Rayleigh-Taylor instabilities in a two-layer liquid film with two deformable interfaces. Here we abstain from the detailed and comprehensive analysis of the system and only focus on the role of the vibration frequency ω for two liquid films as in Fig. 2 swapped around. More precisely, we set $\rho_1 = 785$ kg/m^3, $\rho_2 = 1850$ kg/m^3, $d_1 = 5$ mm, $d_2 = 6$ mm, and $\sigma_2 = 0.015$ N/m, according to [20].

In the vibration-free system, i.e., for $a = 0$, we solve Eq. (28) to determine the complex growth rate λ of the surface deformations as a function of the wave vector k (as in Fig. 2). The system is linearly unstable for longer waves with $0 < k < k_c$, where the cutoff wave vector $k_c = \sqrt{(\rho_2 - \rho_1)g/\sigma_1}$ is independent of the thicknesses of the layers and coincides with the cutoff wave vector for the system with a semi-infinite upper layer [4]. We find that for $0 < k < k_c$, the growth rate λ is strictly real, implying that the Rayleigh-Taylor instability is monotonic. Note that $k_c = \sqrt{(\rho_2 - \rho_1)g/\sigma_1}$ can be found analytically from Eqs. (28) and (A2) by setting $\mathrm{Re}(\lambda)(k_c) = \mathrm{Im}(\lambda)(k_c) = 0$.

The positive part of the growth rate $\lambda = \mathrm{Re}(\lambda)$ vs k is shown by the solid line in Fig. 7. The Rayleigh-Taylor instability is always of the zigzag type, as schematically shown in the insets in Fig. 7 for three selected values of k, indicated by the arrows.

The comparison with the growth rate λ_{LW}, predicted by the zero Reynolds number long-wave approximation [24,25]

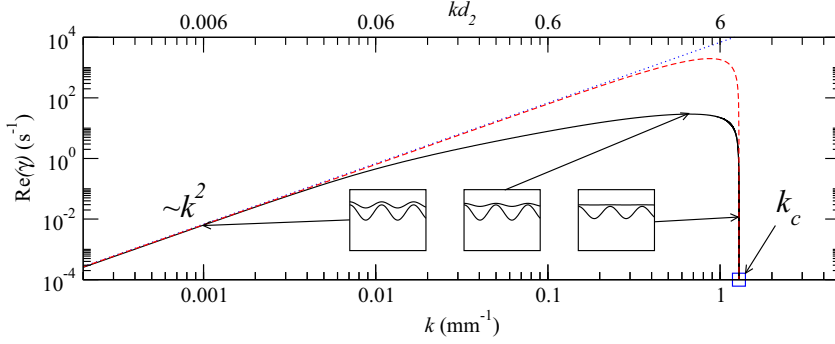$$\lambda(k)_{\mathrm{LW}} = \mathrm{tr}(k)/2 + \sqrt{\mathrm{tr}(k)^2/4 - \det(k)}, \tag{34}$$

FIG. 7. Positive part of the growth rate Re(λ) vs k for a Rayleigh-Taylor unstable two-layer liquid film. The two liquids in Fig. 2 are interchanged with the film thicknesses $d_1 = 5$ mm and $d_2 = 6$ mm and $\sigma_2 = 0.015$ N/m. Insets schematically show the mode type for three different values of k, as indicated by the arrows. Surface perturbations with $k < k_c = \sqrt{(\rho_2 - \rho_1)g/\sigma_1}$ are linearly unstable. Here Re(λ) $\sim k^2$, at small k, as indicated by the dotted line. The dashed line corresponds to the long-wave approximation (34).

with $\det(k) = k^4[(d_2 - d_1)^3 d_1^3 \mu_1^{-1} \mu_2^{-1}/9 + d_1^4 (d_2 - d_1)^2 \mu_1^{-2}/12][\sigma_1 k^2 + (\rho_1 - \rho_2)g](\sigma_2 k^2 + \rho_2 g)$ and $\text{tr}(k) = -k^2\{[\sigma_1 k^2 + (\rho_1 - \rho_2)g]d_1^3 \mu_1^{-1}/3 + (\sigma_2 k^2 + \rho_2 g)[(d_2 - d_1)^3(\mu_2^{-1} - \mu_1^{-1})/3 + d_2^3 \mu_1^{-1}/3]\}$, is instructive. The long-wave approximation (34) is shown by the dashed line in Fig. 7. It correctly predicts the cutoff wave vector k_c, as well as the asymptotic behavior $\lambda(k) \sim k^2$ at small values of k. The agreement with the exact result is further improved when $\rho_2 \to \rho_1$. In this case, the cutoff $k_c \to 0$, implying that the onset of the Rayleigh-Taylor instability is always of the long-wave nature.

Finally, we examine the influence of external vertical vibrations on the Rayleigh-Taylor unstable two-layer film. For different vibration frequencies ω, we plot in Fig. 8 the marginal stability
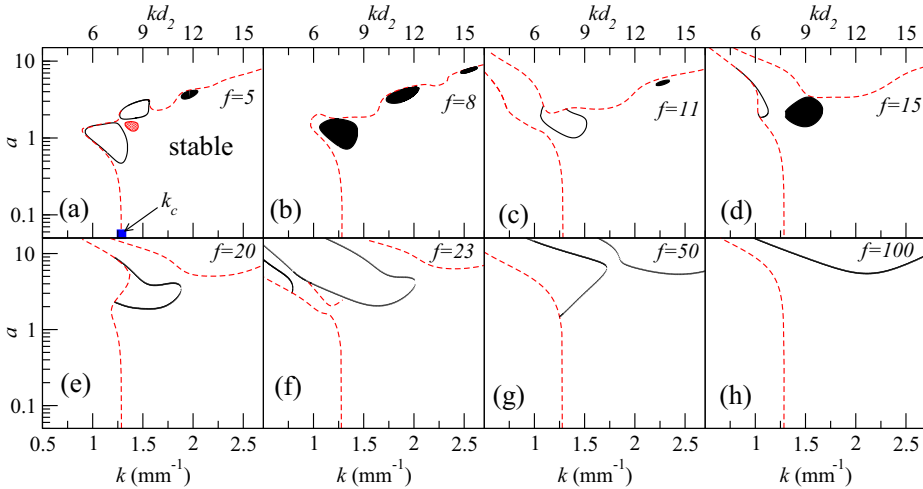

FIG. 8. Rayleigh-Taylor unstable two-layer liquid film under external vertical vibration with parameters as in Fig. 7. Marginal stability curves in the plane of (k,a) for (a) $f = 5$ Hz ($L_1 = 13.1$ and $L_2 = 1.1$), (b) $f = 8$ Hz ($L_1 = 16.6$ and $L_2 = 1.3$), (c) $f = 11$ Hz ($L_1 = 19.4$ and $L_2 = 1.6$), (d) $f = 15$ Hz ($L_1 = 22.7$ and $L_2 = 1.8$), (e) $f = 20$ Hz ($L_1 = 26.2$ and $L_2 = 2.1$), (f) $f = 23$ Hz ($L_1 = 28.1$ and $L_2 = 2.3$), (g) $f = 50$ Hz ($L_1 = 41.4$ and $L_2 = 3.3$), and (h) $f = 100$ Hz ($L_1 = 58.5$ and $L_2 = 4.7$). The stable area stretches to the right from the critical $k_c = \sqrt{(\rho_2 - \rho_1)g/\sigma_1}$, as marked in (a). Filled areas represent isolated islands of unstable parameters: harmonic (heavily filled islands) and subharmonic [lightly filled island in (a)].

curves in the plane (k,a), as obtained from Eq. (25). Dashed (solid) lines correspond to harmonic (subharmonic) stability tongues. For small amplitude $a \ll 1$ and arbitrary frequency ω, the vibration barely changes the stability of the system, with the unstable band of the wave vectors stretching between $k = 0$ and $k = k_c$. At $a \ll 1$, the Rayleigh-Taylor instability sets in at $k \approx k_c$ with the frequency of the external vibration ω (harmonic tongue). As the amplitude a increases, the harmonic stability boundary bends towards smaller values of k, thus confirming that the Faraday instability counterbalances the Rayleigh-Taylor instability and stabilizes the system. This is similar to what was found for the system with one liquid-liquid interface [5].

At relatively small vibration frequencies, we find isolated instability islands, shown by the shaded areas in Fig. 8. Heavily (lightly) shaded areas correspond to isolated subharmonic (harmonic) islands. The islands are located very close to the boundary of the harmonic stability tongue, in some cases intersecting with it, as in Figs. 8(a) and 8(c). In this frequency range, the acoustic length in the upper layer is comparable to its thickness $d_2 - d_1$, i.e., $L_2 \approx 1$. As the frequency ω is gradually increased, the islands appear, move, shrink, and coalesce as illustrated in Fig. 8. We point out the appearance of gaps in the unstable region that protrude towards small k and large values of a. Thus, the first such gap develops at $\omega = 8, \dots, 11$ Hz and the second appears at $\omega = 20, \dots, 23$ Hz. At very large frequencies $\omega = 100$ Hz, the first harmonic tongue is well separated from the first subharmonic tongue, leaving a wide stability gap in between.

VI. CONCLUSION

We have studied the onset of the Faraday instability in a two-layer film that consists of two layers of immiscible viscous fluids on top of each other, supported by a vibrating solid plate. The linearized hydrodynamic equations and the boundary conditions were solved to eliminate the fluid velocities and pressure fields in each layer. The stability condition of the system was reduced to a generalized eigenvalue problem, with the eigenvector that represents the oscillating standing surface wave at the onset of the instability. By numerically solving the eigenvalue problem, we located the stability threshold in the vibrated system. As a side result of our analysis, we also determined the dispersion relation and the decay rates of the surface waves in the vibration-free system.

By considering the relative displacements of the two interfaces, we characterized the surface waves by their mode type. The in phase and the antiphase displacements correspond to the zigzag (barotropic) mode and the varicose thinning mode, respectively. In the vibrated two-layer film both modes are strongly coupled similar to the waves excited in a viscoelastic sheet with two free interfaces [19]. In a two-layer film the mode type is generally time dependent: It changes several times between the in-phase and the anti-phase configuration over one oscillation cycle. A time-dependent mode type is found for both the harmonic and the subharmonic perturbations.

In the absence of vibration and for the fluid parameters as in Refs. [20–22], we found a normal dispersion relation of the surface waves, with a monotonically increasing oscillation frequency as a function of the wave vector. The waves that are shorter than a certain critical wave length are dispersive. Longer waves are monotonically stable, in agreement with the prediction of the zero-Reynolds-number long-wave theory [24,25]. We found two branches of the dispersive surface waves: the least stable zigzag wave and a more stable varicose wave. In extremely short waves, one of the interfaces (liquid-liquid or liquid-gas) is almost flat, making the notion of the mode type of the wave irrelevant. The least stable waves propagate at the upper liquid-gas interface with the liquid-liquid interfaces remaining almost flat.

In the case when the interfacial surface tension between the two liquids is substantially decreased, we find an anomalous dispersion relation of the varicose thinning wave. The short-wavelength varicose mode propagates almost exclusively at the liquid-liquid interface, with the upper surface of the two-layer film remaining almost flat. Varicose waves shorter than a certain critical wavelength are monotonically damped in agreement with an earlier study of the gravity-capillary waves at the interface between two semi-infinite fluids [6].

The capability of our semianalytic approach was further demonstrated by computing the stability tongues in the space spanned by the wave vector of the wave and the vibration amplitude. We consider both the stable case of a lighter fluid on top of the heavier fluid (Fig. 4) and the case of the Rayleigh-Taylor unstable two-layer film, with a heavier fluid on top of the lighter fluid (Figs. 5 and 6). One remarkable feature of the Rayleigh-Taylor unstable system under vibration is the existence of isolated islands of unstable parameters in the stability diagram. These islands are observed at low frequencies for a high-viscosity fluid on top of a low-viscosity fluid.

ACKNOWLEDGMENT

APPENDIX

The matrix $\boldsymbol{M}$ in Eq. (23) is given by

$$\boldsymbol{M} = \begin{pmatrix} 1 & 1 & 1 & 1 \\ k & -k & q_1 & -q_1 \\ e^{kd_1} & e^{-kd_1} & e^{q_1 d_1} & e^{-q_1 d_1} \\ ke^{kd_1} & -ke^{-kd_1} & q_1 e^{q_1 d_1} & -q_1 e^{-q_1 d_1} \\ 2\mu_1 k^2 e^{kd_1} & 2\mu_1 k^2 e^{-kd_1} & \mu_1(k^2+q_1^2)e^{q_1 d_1} & \mu_1(k^2+q_1^2)e^{-q_1 d_1} \\ e^{kd_1} & e^{-kd_1} & e^{q_1 d_1} & e^{-q_1 d_1} \\ 0 & 0 & 0 & 0 \\ 0 & 0 & 0 & 0 \end{pmatrix}$$

$$\begin{pmatrix} 0 & 0 & 0 & 0 \\ 0 & 0 & 0 & 0 \\ -e^{kd_1} & -e^{-kd_1} & -e^{q_2 d_1} & -e^{-q_2 d_1} \\ -ke^{kd_1} & ke^{-kd_1} & -q_2 e^{q_2 d_1} & q_2 e^{-q_2 d_1} \\ -2\mu_2 k^2 e^{kd_1} & -2\mu_2 k^2 e^{-kd_1} & -\mu_2(k^2+q_2^2)e^{q_2 d_1} & -\mu_2(k^2+q_2^2)e^{-q_2 d_1} \\ 0 & 0 & 0 & 0 \\ 2k^2 e^{kd_2} & 2k^2 e^{-kd_2} & (k^2+q_2^2)e^{q_2 d_2} & (k^2+q_2^2)e^{-q_2 d_2} \\ e^{kd_2} & e^{-kd_2} & e^{q_2 d_2} & e^{-q_2 d_2} \end{pmatrix}. \quad (A1)$$

For any $\lambda + I\omega n/2 \neq 0$ the coefficients $A_{ik}^{(n)}$ in Eq. (24) are given by

$$\begin{aligned} A_{11}^{(n)} &= \left[\rho_1\left(\frac{I\omega n}{2}+\lambda\right)+3\mu_1 k^2\right](D_1 ke^{kd_1}-D_2 ke^{-kd_1}+q_1 D_3 e^{q_1 d_1}-q_1 D_4 e^{-q_1 d_1}) \\ &\quad -\mu_1(D_1 k^3 e^{kd_1}-D_2 k^3 e^{-kd_1}+q_1^3 D_3 e^{q_1 d_1}-q_1^3 D_4 e^{-q_1 d_1}) \\ &\quad -\left[\rho_2\left(\frac{I\omega n}{2}+\lambda\right)+3\mu_2 k^2\right](D_5 ke^{kd_1}-D_6 ke^{-kd_1}+q_2 D_7 e^{q_2 d_1}-q_2 D_8 e^{-q_2 d_1}) \\ &\quad +\mu_2(D_5 k^3 e^{kd_1}-D_6 k^3 e^{-kd_1}+q_2^3 D_7 e^{q_2 d_1}-q_2^3 D_8 e^{-q_2 d_1}) \\ &\quad +\gamma_1 k^4 +(\rho_1-\rho_2)g_0 k^2, \\ A_{21}^{(n)} &= \left[\rho_2\left(\frac{I\omega n}{2}+\lambda\right)+3\mu_2 k^2\right](D_5 ke^{kd_2}-D_6 ke^{-kd_2}+q_2 D_7 e^{q_2 d_2}-q_2 D_8 e^{-q_2 d_2}) \\ &\quad -\mu_2(D_5 k^3 e^{kd_2}-D_6 k^3 e^{-kd_2}+q_2^3 D_7 e^{q_2 d_2}-q_2^3 D_8 e^{-q_2 d_2}), \\ A_{12}^{(n)} &= \left[\rho_1\left(\frac{I\omega n}{2}+\lambda\right)+3\mu_1 k^2\right](E_1 ke^{kd_1}-E_2 ke^{-kd_1}+q_1 E_3 e^{q_1 d_1}-q_1 E_4 e^{-q_1 d_1}) \\ &\quad -\mu_1(E_1 k^3 e^{kd_1}-E_2 k^3 e^{-kd_1}+q_1^3 E_3 e^{q_1 d_1}-q_1^3 E_4 e^{-q_1 d_1}) \end{aligned}$$

$$-\left[\rho_2\left(\frac{I\omega n}{2}+\lambda\right)+3\mu_2 k^2\right]\left(E_5 k e^{kd_1}-E_6 k e^{-kd_1}+q_2 E_7 e^{q_2 d_1}-q_2 E_8 e^{-q_2 d_1}\right)$$

$$+\mu_2\left(E_5 k^3 e^{kd_1}-E_6 k^3 e^{-kd_1}+q_2^3 E_7 e^{q_2 d_1}-q_2^3 E_8 e^{-q_2 d_1}\right),$$

$$A_{22}^{(n)}=\left[\rho_2\left(\frac{I\omega n}{2}+\lambda\right)+3\mu_2 k^2\right]\left(E_5 k e^{kd_2}-E_6 k e^{-kd_2}+q_2 E_7 e^{q_2 d_2}-q_2 E_8 e^{-q_2 d_2}\right)$$

$$-\mu_2\left(E_5 k^3 e^{kd_2}-E_6 k^3 e^{-kd_2}+q_2^3 E_7 e^{q_2 d_2}-q_2^3 E_8 e^{-q_2 d_2}\right)$$

$$+\gamma_2 k^4+\rho_2 g_0 k^2. \tag{A2}$$

For $\lambda+I\omega n/2=0$ Eq. (A2) is applied by setting $E_i=D_i=0$.

---

[1] M. Faraday, On a peculiar class of acoustical figures; and on certain forms assumed by groups of particles upon vibrating elastic surfaces, Philos. Trans. R. Soc. London **121**, 299 (1831).

[2] S. Chandrasekhar, *Hydrodynamic and Hydromagnetic Stability* (Dover, New York, 1981).

[3] K. Kumar and L. S. Tuckerman, Parametric instability of the interface between two fluids, J. Fluid Mech. **279**, 49 (1994).

[4] S. G. Yiantsios and B. G. Higgins, Rayleigh-Taylor instability in thin viscous films, Phys. Fluids A **1**, 1484 (1989).

[5] V. Lapuerta, F. J. Mancebo, and J. M. Vega, Control of Rayleigh-Taylor instability by vertical vibration in large aspect ratio containers, Phys. Rev. E **64**, 016318 (2001).

[6] U.-S. Jeng, L. Esibov, L. Crow, and A. Steyerl, Viscosity effect on capillary waves at liquid interfaces, J. Phys.: Condens. Matter **10**, 4955 (1998).

[7] F. M. Hoffmann and G. H. Wolf, Excitation of parametric instabilities in statically stable and unstable fluid interfaces, J. Appl. Phys. **45**, 3859 (1974).

[8] F. Troyon and R. Gruber, Theory of the dynamic stabilization of the Rayleigh-Taylor instability, Phys. Fluids **14**, 2069 (1971).

[9] K. Kumar, Linear theory of faraday instability in viscous liquids, Proc. R. Soc. London A **452**, 1113 (1996).

[10] S. T. Milner, Square patterns and secondary instabilities in driven capillary waves, J. Fluid Mech. **225**, 81 (1991).

[11] J. Miles, On Faraday waves, J. Fluid Mech. **248**, 671 (1993).

[12] H. W. Müller, H. Wittmer, C. Wagner, J. Albers, and K. Knorr, Analytic Stability Theory for Faraday Waves and the Observation of the Harmonic Surface Response, Phys. Rev. Lett. **78**, 2357 (1997).

[13] M. Bestehorn and I. D. Borcia, Thin film lubrication dynamics of a binary mixture: Example of an oscillatory instability, Phys. Fluids **22**, 104102 (2010).

[14] M. Bestehorn, Q. Han, and A. Oron, Nonlinear pattern formation in thin liquid films under external vibrations, Phys. Rev. E **88**, 023025 (2013).

[15] M. Bestehorn, Laterally extended thin liquid films with inertia under external vibrations, Phys. Fluids **25**, 114106 (2013).

[16] J. Rajchenbach and D. Clamond, Faraday waves: Their dispersion relation, nature of bifurcation and wavenumber selection revisited, J. Fluid Mech. **777**, R2 (2015).

[17] J. P. Embs, C. Wagner, K. Knorr, and M. Lücke, Measuring the anomalous dispersion branch of surface waves on ferrofluids, Europhys. Lett. **78**, 44003 (2007).

[18] S. Kumar, Parametrically driven surface waves in viscoelastic liquids, Phys. Fluids **11**, 1970 (1999).

[19] S. Kumar, Parametric instability of a liquid sheet, Proc. R. Soc. London A **457**, 1315 (2001).

[20] G. Pucci, E. Fort, M. Ben Amar, and Y. Couder, Mutual Adaptation of a Faraday Instability Pattern with its Flexible Boundaries in Floating Fluid Drops, Phys. Rev. Lett. **106**, 024503 (2011).

[21] G. Pucci, M. Ben Amar, and Y. Couder, Faraday instability in floating liquid lenses: The spontaneous mutual adaptation due to radiation pressure, J. Fluid Mech. **725**, 402 (2013).

[22] G. Pucci, M. Ben Amar, and Y. Couder, Faraday instability in floating drops, Phys. Fluids **27**, 091107 (2015).

[23] L. D. Landau and E. M. Lifshitz, *Fluid Mechanics*, 2nd ed. (Pergamon, Oxford, 1987), Vol. 6.

[24] A. Pototsky, M. Bestehorn, D. Merkt, and U. Thiele, Alternative pathways of dewetting for a thin liquid two-layer film, Phys. Rev. E **70**, 025201(R) (2004).

[25] A. Pototsky, M. Bestehorn, D. Merkt, and U. Thiele, Morphology changes in the evolution of liquid two-layer films, J. Chem. Phys, **122**, 224711 (2005).

[26] O. M. Phillips, *The Dynamics of the Upper Ocean* (Cambridge University Press, Cambridge, 1980).

[27] A. Oron and P. Rosenau, Nonlinear evolution and breaking of interfacial Rayleigh-Taylor waves, Phys. Fluids A **1**, 1155 (1989).

[28] A. Oron and P. Rosenau, Formation of patterns induced by thermocapillarity and gravity, J. Phys. (France) II **2**, 131 (1992).

[29] G. H. Wolf, The dynamic stabilization of the Rayleigh-Taylor instability and the corresponding dynamic equilibrium, Z. Phys. **227**, 291 (1969).

[30] G. H. Wolf, Dynamic Stabilization of the Interchange Instability of a Liquid-Gas Interface, Phys. Rev. Lett. **24**, 444 (1970).